

FocusLLaVA: A Coarse-to-Fine Approach for Efficient and Effective Visual Token Compression

Yuke Zhu^{1*}, Chi Xie^{2*}, Shuang Liang², Bo Zheng¹, Sheng Guo¹

¹Mybank, Ant Group ²Tongji University

{felix.yk, guangyuan, guosheng.guosheng}@mybank.cn {chixie, shuangliang}@tongji.edu.cn

Abstract

Recent advances on Multi-modal Large Language Models have demonstrated that high-resolution image input is crucial for model capabilities, especially for fine-grained tasks. However, high-resolution images lead to a quadratic increase in the number of visual tokens input into LLMs, resulting in significant computational costs. Current work develop visual token compression methods to achieve efficiency improvements, often at the expense of performance. We argue that removing visual redundancy can simultaneously improve both efficiency and performance. We build a coarse-to-fine visual token compression method, with a vision-guided sampler for compressing redundant regions with low information density, and a text-guided sampler for selecting visual tokens that are strongly correlated with the user instructions. With these two modules, the proposed FocusLLaVA achieves improvements in both efficiency and performance. We validate the effectiveness of our approach on a wide range of evaluation datasets.

1. Introduction

Recently, the study of Multimodal Large Language Models (MLLMs) has attracted considerable attention from researchers. With a variety of MLLMs like LLaVA [33, 34] being proposed, significant progress has been made in this field. One of the major improvement for recent MLLMs is the support for high-resolution images. Early works [25, 33] use a fixed, small input scale, regardless of the original image size. This process inevitably led to the loss of image details, making the model incapable of handling tasks that require fine-grained image understanding. Recently, supporting high-resolution image input [3, 28] has become a common interest in the industry. However, high-resolution images lead to a quadratic increase in the number of visual tokens in the LLM, resulting in increased inference time and higher memory consumption.

To address the problem, numerous studies have focused on reducing the number of visual tokens in high-resolution images. However, most of these methods employ a heuristic approach for visual token compression [2, 5, 45, 54]. They leverage hand-crafted metrics to filter out tokens, which often at the price of the performance. Some other works [25, 51, 54] design query transformers to compress image information into a fixed number of queries, which lead to information loss for detailed images and sometimes a complex training scheme. Generally, current approach cannot guarantee maintaining model performance while reducing visual tokens. They focus on achieving a trade-off between faster speed and less performance loss.

In this paper, we propose *FocusLLaVA*, which removes visual redundancy and simultaneously improves both performance and efficiency. It uses a coarse-to-fine approach for this target: it first compress low information density features based on visual information (**Vision-Guided Sampler**), and then select tokens relevant to the query based on textual instructions (**Text-Guided Sampler**).

We make several technical designs for these two modules. First, the **region-level compression** in vision-guided sampler: it down-samples each local region with multiple scales and select one of them adaptively. We use regions rather than token as the basic units to enables a multi-scale manner, which is more flexible. Second, the **disentangled compression** of the two samplers: the vision-guided sampler is placed in the projector, as it requires only image information and serves as a coarse step for reducing redundant tokens early. In contrast, the text-guided sampler is integrated within the intermediate layers of the LLM, as it necessitates stronger language features to pinpoint areas related to the instructions. Third, a straightforward, one-step **training recipe** carefully designed for both modules. For the former, we use an auxiliary balance loss to encourage the vision-guided sampler to explore various scales. For the latter, we design a stochastic training technique to adapt the LLM to token changes. The fine-tuning step is one-stage, as the baseline.

To validate the effectiveness of *FocusLLaVA*, we con-

*Equal contribution.

duct experiments on various mainstream multimodal evaluation benchmarks. The results demonstrate that our approach not only optimizes the inference speed, but also improves performance. With 39% visual tokens, *FocusLLaVA* outperforms the baseline method in a wide range of benchmarks. In summary, the main contributions of our work can be summarized as follows:

1. We propose *FocusLLaVA*, a novel coarse-to-fine approach for visual token reduction, which leverages the guidance from both visual and textual information.
2. We carefully designed two modules, the vision-guided sampler and the text-guided sampler, along with a complete training methodology.
3. We demonstrate both efficiency and performance improvements of *FocusLLaVA* on broad benchmarks. It shows highly competitive results compared to SOTA MLLMs. Extensive experiments are conducted for better understanding of both visual and textual guidance.

2. Related Work

MLLMs. Early models like BLIP2 [25] and Instruct-BLIP [14] designed a Q-Former to bridge encoded visual information into the input space of LLMs. These approaches typically require complex training processes to train the image-text alignment module. Methods represented by Flamingo [1] proposed incorporating encoded image information into LLM layers using cross-attention. Fuyu8B [4] entirely discarded the visual encoder, directly inputting image patches into the LLM. LLaVA [33], on the other hand, uses an MLP layer to directly bridge encoded image information into the LLM’s input space, making the model architecture and training process much more straightforward. Consequently, many subsequent multimodal large models have made improvements based on LLaVA [7, 18, 29, 34, 35]. For instance, LLaVA 1.5 [34] optimized data quality, while LLaVA-Next [35] introduced adaptive image segmentation techniques to support high-resolution images.

High-resolution MLLM. Recently, various MLLMs have adopted high-resolution images as input to capture fine-grained image information. In the early stages, most MLLMs use a fixed size of 224 for their inputs. LLaVA-1.5 [34] and BLiVA [19] increased the image size to 336 to achieve better performance. Qwen-VL [3] expanded the size further to 448. It first trained with a fixed image scale of 224 and then fine-tuned by increasing the resolution to 448. Vary [47] and Mini-Gemini [27] additionally introduced a Vision Encoder specifically for high-resolution images. SPHINX [31], Monkey [28], and LLaVA-UHD [48] resize the images to a fixed resolution and then split them into several patches. These patches are individually encoded before being fed to the LLM. Furthermore, LLaVA-NeXT [30] employs a series of predefined resolutions, first matching the

input image to the closest resolution, and then segmenting it into sub-images. Qwen2-VL [46] directly uses the original resolution of the image and encodes it into dynamically variable-length visual tokens by modifying the structure of ViT [15]. LLaVA-HR [39], LLaVA-M3 [5], and Dragonfly [10] advocate for the use of multi-scale information to enhance MLLM capabilities. They resize the original images into multiple resolutions, each encoded individually, and then feed them into the LLM. This approach leverages the benefits of different scales, providing a more comprehensive representation of the input data.

Visual token compression. In the field of MLLM, the works for visual token compression can be broadly categorized into three types. The first type [51, 52, 54] employs a QFormer-like [14, 25] structure to compress visual tokens. However, they heavily rely on the quality of alignment between image and text, necessitating a complex training process for alignment. Subsequent works, such as QwenVL [3], employ a single layer of cross-attention to replace QFormer, thereby reducing the training complexity. However, it still uses a fixed number of queries for image information compression, which leads to information loss, especially in tasks requiring fine-grained information. The second category [6, 10, 24, 37, 43, 45, 53] leverages manually designed techniques for compressing image information. For instance, LLaVA-PruMerge [43] dynamically identifies and retains the most critical visual tokens, then merges similar ones through clustering. TextMonkey [37] performs compression based on token similarity. HiRED [2] utilizes the attention map from the CLS token of ViT to discard unimportant tokens. These approaches rely on handcrafted metrics to gauge the importance of visual tokens, which does not guarantee optimal performance in terms of model accuracy. In contrast, our proposed method adopts a learning-based approach that allows the model to select the most appropriate visual scale for each local region. The selection is directly linked to the model’s global optimization objective. The third category [13, 32], directly applies token pruning methods from LLMs to the selection of visual tokens. These methods do not effectively utilize the inherent information. Moreover, the primary focus of these works is on enhancing computational efficiency, with less emphasis on the performance.

3. Method

The proposed *FocusLLaVA* is designed with two objectives: (i) fully leverage visual and textual information to effectively reduce the number of visual tokens for efficiency improvement; (ii) enable the model to learn to remove redundant visual information in a coarse-to-fine manner for performance improvement.

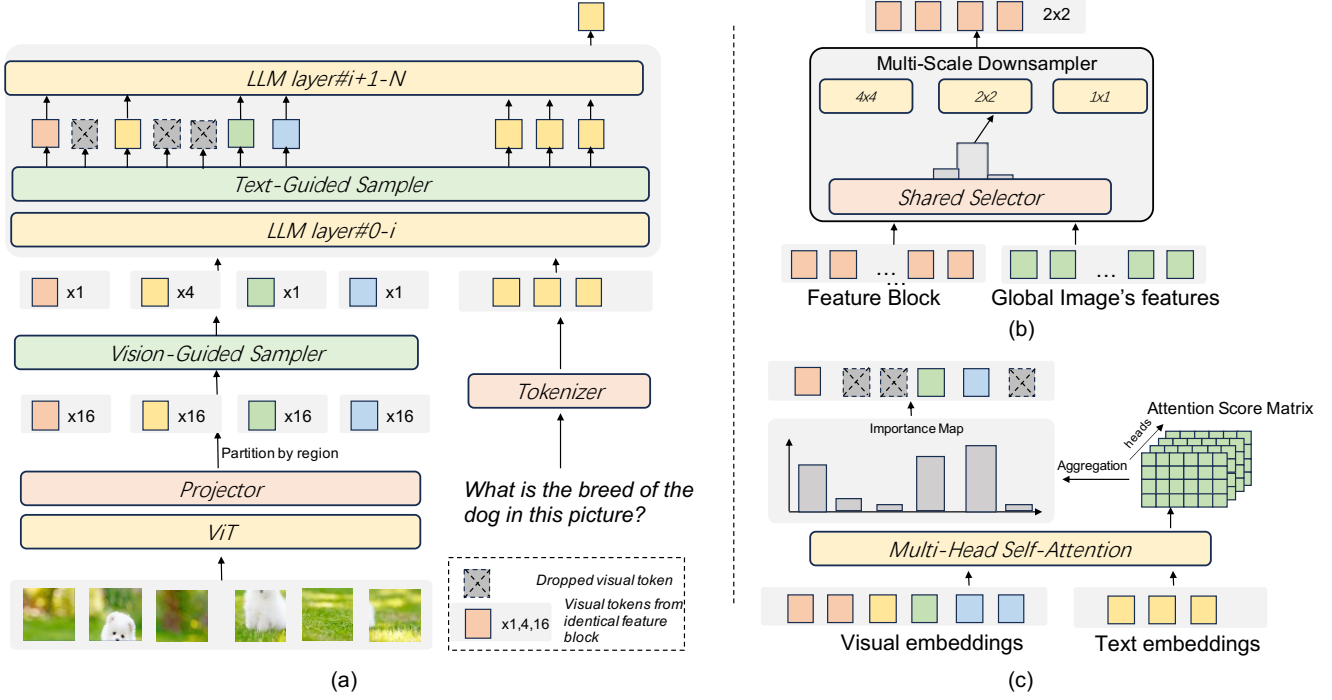


Figure 1. (a) **Overall structure of FocusLLaVA.** The two core modules are vision-guided sampler and text-guided sampler. The features from each sub-images are first concatenated into a whole and then partitioned by regions, each forming a local feature block. It is then processed by vision-guided sampler. (b) **The structure of vision-guided sampler.** It takes a feature block and global image’s features as inputs and output the predicted sampling scale for this region. (c) **The structure of text-guided sampler.** It aggregates the multi-head attention scores to form the importance map of visual tokens.

3.1. Overall Structure

The overall structure of the proposed model is illustrated in Fig. 1. We build our model based on the LLaVA-Next [30] with two core modules, vision-guided sampler and text-guided sampler inserted in the projector and LLM respectively. The vision-guided sampler selects visual tokens based on the image information itself, while the latter combines textual information to provide stronger semantic guidance, filtering visual tokens relevant to user instructions.

For a given image $\mathbf{I} \in \mathbb{R}^{H \times W \times 3}$ with high resolution, we follow LLaVA-Next to first segment the image into several local sub-images. The segmented sub-images, along with the original image, are resized to a uniform size to form an image sequence $[\mathbf{I}_g, \mathbf{I}_0, \mathbf{I}_1, \mathbf{I}_2, \dots, \mathbf{I}_{N-1}]$, where \mathbf{I}_g is the resized image block of the original image and N is the total number of local sub-images. Each image in the sequence is encoded by ViT independently. The results are then passed through a projector, resulting in a set of image embeddings that are aligned with LLM’s embedding space. Each image embedding is also called a visual token. Then, we concatenate and reshape all visual tokens from all sub-images to form a global feature map, referred as $\mathbf{X} \in \mathbb{R}^{H_x \times W_x \times C}$. Subsequently, the vision-guided sam-

pler performs visual token reduction for the feature map, with the remaining tokens inputted into the LLM. Within the LLM, a second round of selection is performed by the text-guided sampler, resulting in a set of visual tokens that are precisely correlated with text instruction.

3.2. Vision-Guided Sampler

For the global feature map \mathbf{X} , it is first partitioned by region to form a set of local feature blocks $\mathbf{X}_0, \mathbf{X}_1, \dots, \mathbf{X}_{M-1}$, where M is the number of local feature blocks. We denote the region’s window size as w . Each feature block $\mathbf{X}_i \in \mathbb{R}^{w \times w \times C}$ serves as the basic unit for vision-guided sampler. Note that the selection of visual scales is performed for each local region rather than the entire feature map. This design allows for adaptive scale selection for each local area of high-resolution images. The vision-guided sampler processes feature block in two steps. First, it down-samples each feature block to multiple different scales. Then, it dynamically selects one of the visual scales based on the local information and global information.

Multi-scale down-sampling. For each of the feature block $\mathbf{X}_i \in \mathbb{R}^{w \times w \times C}$, we use a set of Max-Pooling operations to down-sample it into several different scales. In our work,

we use a window size of 4 to partition the feature map, resulting in $\mathbf{X}_i \in \mathbb{R}^{4 \times 4 \times C}$. We use three max-pooling operations, each with size 4×4 , 2×2 , and 1×1 to process the feature block, resulting in three kinds of token set for this feature block: $\text{DS}[0](\mathbf{X}_i) \in \mathbb{R}^{1 \times 1 \times C}$, $\text{DS}[1](\mathbf{X}_i) \in \mathbb{R}^{2 \times 2 \times C}$, and $\text{DS}[2](\mathbf{X}_i) \in \mathbb{R}^{4 \times 4 \times C}$, where $\text{DS}[i]$ denotes the i -th down-sampling type. The design of max-pooling operations can be more flexible. For example, we can use unsymmetrical pooling with ratio 2 or $\frac{1}{2}$ to get more kinds of token set. We will discuss this design in the experiments.

Multi-scale selection. We adopt the design concept of Mixture of Experts (MoE), treating multiple scales of down-sampling as experts. The goal is to select one expert for each local feature block. To achieve this, we design a multi-scale selector by modeling the correlation between each local feature block and the global context. Specifically, we use the scaled original image as \mathbf{I}_g and its encoded features as \mathbf{X}_g . We flatten \mathbf{X}_g to make $\mathbf{X}_g \in \mathbb{R}^{H_x W_x \times C}$. Then, each basic feature block \mathbf{X}_i is pooled to $1 \times 1 \times C$, which is used to calculate the inner product with \mathbf{X}_g as $\text{Score}_i = \text{pool}(\mathbf{X}_i)^T \mathbf{X}_g$, where $\text{Score}_i \in \mathbb{R}^{1 \times H_x W_x}$. Subsequently, a fully connected layer is applied to Score_i to predict the scale of each feature block, producing logits $\mathbf{Z} \in \mathbb{R}^{1 \times S}$ for visual scale selection. Finally, we apply the softmax function to calculate the probabilities of each visual scale. The tokens corresponding to the visual scale with the highest probability are then input to the LLM.

Objective. Due to the non-differentiable nature of the selection operation in the down-sampling paths, the parameters of the selector cannot be effectively trained. To fix this, we introduce some techniques. Given a local base feature block \mathbf{X}_r , we use $\text{DS}[i]$ to denote the i -th down-sampling path. The final visual token corresponding to \mathbf{X}_r that is ultimately selected and input into the LLM is

$$\tilde{\mathbf{X}}_r = \text{DS}[\text{argmax}(\mathbf{Z})](\mathbf{X}_r), \quad (1)$$

where \mathbf{Z} is the predicted logits corresponding to \mathbf{X}_r . During inference, we apply the multi-scale selection using the aforementioned formula. While during training, we multiply the calculated probability with the tokens to make the entire process differentiable. Specifically:

$$\tilde{\mathbf{X}}_r = \text{Top1}(\text{Softmax}(\mathbf{Z})) * \text{DS}[\text{argmax}(\mathbf{Z})](\mathbf{X}_r). \quad (2)$$

In this way, the probability calculated in the sidetrack is incorporated into the token, allowing the parameters of the selector to continue receiving gradient feedback through the LLM’s optimization loss. Furthermore, we observed that the selector tends to easily degrade into a trivial state where it continuously selects one particular branch during the training process. To counteract the laziness of network optimization, we follow switch-transformer [16] to introduce a balance loss to force the network to choose different

branches. The form of the balance loss is as follows:

$$L_{\text{balance}} = \alpha \sum_0^n f_i * P_i, \quad (3)$$

$$f_i = \frac{1}{N} \sum_0^{N-1} \mathbf{1}(\text{argmax}(\mathbf{Z}) = i), \quad (4)$$

$$P_i = \frac{1}{N} \sum_{\mathbf{Z}} \text{Softmax}(\mathbf{Z})_i, \quad (5)$$

where α is the weight of the balance loss and $\text{textbf{1}}$ denotes the indicator function and N denotes the total number of basic feature blocks within one batch.

3.3. Text-Guided Sampler

In text-guided sampler, we utilize the text comprehension capabilities of LLM to serve as the basis for visual token selection. To achieve this, text embeddings from the intermediate layers of LLMs are selected as guidance for visual token filtering. We believe that the text embeddings in the intermediate layers of LLM, which have already interacted with the visual signal, contain sufficient semantic information and have the ability to select important visual tokens. This idea is supported by a further analysis. As shown in Fig. 5, we visualize the attention scores received by each visual token in several layers. We observed that in the shallow layers of the LLM, the importance pattern of visual tokens is unstable and undergoes significant changes. Moreover, the importance map can hardly focus on the most correlated area. In contrast, in the intermediate and deeper layers of the LLM, the importance pattern of visual tokens tends to become consistent and accurate. For this reason, we argue that the text-guided sampler should be placed the middle layers of LLM, rather than shallow layers or out of LLM.

For the i -th layer of the LLM, we first compute the similarity matrix $\mathbf{A}_i \in \mathbb{R}^{h \times N \times T}$ between the text prompt’s embedding \mathbf{h}_i^t and the visual token’s embedding \mathbf{h}_i^v , where h denotes the number of heads in the multi-head attention, N indicates the number of visual tokens, and T represents the number of text prompt tokens:

$$\mathbf{Q}_i = \mathbf{W}_i^q \mathbf{h}_i^t \quad \mathbf{K}_i = \mathbf{W}_i^k \mathbf{h}_i^v \quad (6)$$

$$\mathbf{A}_i = \text{Softmax} \left(\frac{\mathbf{Q}_i \mathbf{K}_i^T}{\sqrt{d}} \right). \quad (7)$$

To determine the importance score \mathbf{S}_i for each visual token, we first employ a reduce-max operation to identify the highest score across all attention heads. Subsequently, we average these importance scores over all textual tokens. After obtaining the importance score \mathbf{S}_i , we select the top- k visual tokens with the highest importance scores for retention. Mathematically, this process can be expressed as:

$$\mathbf{S}_i = \frac{1}{T} \sum_{j=0}^{T-1} \max_h \mathbf{A}_i[h, j], \quad \mathbf{S}_i \in \mathbb{R}^N, \quad (8)$$

where \mathbf{A}_i represents the attention scores for the i -th visual token across all attention heads and textual tokens, T is the total number of textual tokens, and N is the total number of visual tokens. In the selection of significant visual tokens, we first sort \mathbf{S}_i in descending order to obtain $\{s_0, s_1, \dots, s_{N-1}\}$. Then, we select the visual tokens whose cumulative importance exceeds a given threshold,

$$k = \min_j \sum_{i=0}^{j-1} \frac{s_i}{\sum_{i=0}^{N-1} s_i} > \gamma, \quad (9)$$

where γ is the importance threshold. Finally, the top k visual tokens, ranked by the importance, are selected.

In LLMs, filtering visual tokens based on importance typically leads to a decline in model performance. We believe that discarding some tokens in LLMs causes inconsistency between the training and testing. To compensate for the performance degradation, we introduce randomness during the training process to enhance the model’s adaptability. Specifically, during training, for each image-text pair, we can randomly select a decoder layer and an importance threshold γ , and then choose the visual tokens according to the importance formula. The model, after being trained with this randomness-enhanced approach, demonstrates stronger robustness in testing.

4. Experiments

4.1. Implementation Details

We use CLIP [42] ViT-L/14 as the visual encoder (default resolution 336×336), LLama3-8B as the LLM and a 2-layer MLP as the connector. We keep the adaptive image slicing technique used in LLaVA-Next [30] with each sub-image being resized to 336×336 . For the vision-guided sampler, we set the window size of local feature block to 4. Three scales 4×4 , 2×2 and 1×1 are used for multi-scale selection. For the text-guided sampler, we insert it into the 8-th layer in LLM. γ is set to 0.85 by default. During training, it is randomly inserted into layers between 8 and 24. Following LLaVA-Next, we use similar training settings for visual instruction fine-tuning. The learning rate is set to $1e-5$ with a cosine learning rate scheduler and a batch size of 128. The training takes one epoch using AdamW optimizer. Deepspeed Zero2 is used as the training framework. We conduct experiments on a server equipped with 8 Nvidia A100 GPUs, each with 80GB of VRAM.

4.2. Datasets and Benchmarks

Training datasets. We pretrain and fine-tune the proposed model with only open-source data. For pretraining, we follow the popular llava series to use llava-pretrain-558k. For fine-tuning, we have made every effort to align our training data with LLaVA-NeXT [35]. However, as

the tens of thousands of real user data used by LLaVA-NeXT is not released, we follow Open-LLaVA-NeXT [11] to use 200K ALLaVA-Instruct-VFLAN-4V [8] data as a substitute. Additionally, since TextVQA [44] has been included in the training data of most existing LMMs, we retain it to enable fair comparisons with other LMMs. As a result, the fine-tuning data includes 1M samples, covering sharegpt4v-mix665k [12], ALLaVA-Instruct-VFLAN-4V, DocVQA [41], SynDog-EN [23], ChartQA [40], DVQA [21], AI2D [22], and GeoQA+ [9]. The specific data configuration are available in the supplementary.

Benchmarks. We use 10 popular benchmarks to evaluate our method, including (1) General question answering benchmarks such as GQA [20] and ScienceQA [38]; (2) Optical character based visual question answering benchmark such as TextVQA [44]; (3) MLLM benchmarks for specific abilities, like POPE [26], MM-Vet [50] and LLaVA-in-the-wild [33]; (4) Comprehensive MLLM benchmarks such as MME [17] (Perception and Cognition), MMBench [36] and MMBench-CN.

4.3. Performance

We have selected three types of approaches for comparative reference, with their results presented in Tab. 1, separated by different categories. The first type consists of various mainstream MLLMs. The second type includes MLLMs that take high-resolution inputs. The third type focuses on works dedicated to compressing visual tokens, for which we have chosen their best outcomes. The final section presents our baseline and methods. Given that the foundational LLMs, training datasets, and training configurations used in current MLLM research vary, most of the results in Tab. 1 are not directly comparable. However, these results can serve as a reference to illustrate the approximate performance level of our implemented baseline and methods. In the third part, specifically for our self-implemented LLaVA-Next and *FocusLLaVA*, we ensured strict alignment in the foundational large models, training datasets, and training settings, making them fairly comparable. Our findings indicate that our implemented baseline is highly competitive compared to both mainstream and high-resolution MLLMs. Furthermore, our proposed *FocusLLaVA* demonstrates clear improvements over this baseline.

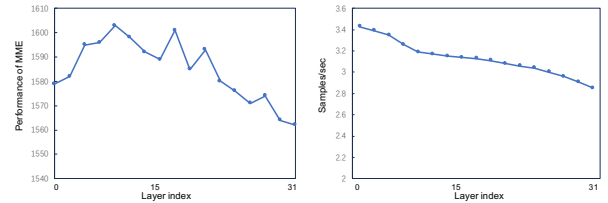


Figure 2. Performance and speed with textual guidance in different layers.

Table 1. **Comparison with existing MLLMs on popular benchmarks.** VQA^T: TextVQA [44]; SQA: ScienceQA [38]; LLaVA^W: LLaVA-bench-in-the-wild; MME^{PC}: Perception and Cognition in MME [17]; MMB^C denotes MMBench-CN [36].

Method	LLM	VQA ^T	SQA	GQA	POPE	MM-Vet	LLaVA ^W	MME ^P	MME ^C	MMB	MMB ^C
Instruct-BLIP [14]	Vicuna-7B	50.1	-	49.2	-	26.2	60.9	1084	229	36.0	23.7
Qwen-VL [3]	Qwen-7B	63.8	-	59.3	-	-	-	1487.6	-	60.6	7.4
LLaVA-1.5 [34]	Vicuna-7B	58.2	-	62.0	85.9	30.5	65.4	1510	-	64.3	58.3
LLaVA-1.5	Llama3-8B	58.9	-	61.9	85.1	34.8	70.5	1544	328	72.9	67.7
mPlugOwl3 [49]	Qwen-8B	69.0	-	65.0	88.2	40.1	-	-	-	77.6	74.3
Otter-HD [24]	Fuyu-8B	-	-	-	86.0	-	-	1223	331	58.30	-
LLaVA-NeXT [35]	Vicuna-7B	64.9	70.1	64.2	86.5	-	-	1519	332	67.4	60.6
Mini-Gemini-HD [27]	Vicuna-7B	68.4	-	-	-	41.3	-	1546	319	65.8	-
SiME [54]	Llama3-8B	64.7	84.2	63.9	-	37.4	73.9	1578	337	75.0	71.8
LLaVA-Prumerge+ [43]	Vicuna-7B	57.1	68.3	-	84.0	-	-	1462	-	64.9	-
Trim [45]	Vicuna-7B	-	69.1	61.4	85.3	28.0	58.7	1461	-	67.4	54.9
HiRED [2]	Vicuna-13B	65.2	73.2	-	87.7	-	-	1570	-	-	-
LLaVA-NeXT (Ours)	Llama3-8B	69.4	77.3	65.7	86.9	40.6	64.7	1558	334	74.2	70.1
FocusLLaVA (Ours)	Llama3-8B	70.0	79.0	66.0	87.7	41.3	65.6	1600	328	74.7	70.3

Table 2. **Ablation on visual and textual guidance.** “Vision tokens” means the percentage of visual tokens remained. “Speed” means number of samplers per second. The speed is tested on TextVQA [44].

Setting	Vision tokens	Speed	TextVQA	MME	ScienceQA	GQA
Baseline	100%	2.85	65.5	1562	76.4	61.7
Vision	49%	3.76	65.2	1590	77.8	62.3
Text	81%	3.19	65.4	1603	76.9	62.1
Both	39%	4.01	65.9	1597	78.1	62.6

4.4. Analysis

For experiments in this part, a smaller training set (200K) is used for convenience. It is randomly sampled from the default training set.

Ablation on visual and textual guidance. We experiment to explore the individual contribution of vision-guided sampler and text-guided sampler. The results are presented in Tab. 2. The findings indicate that both the vision-guided sampler and the text-guided sampler help the model improve performance across multiple evaluation benchmarks. When combined, they further enhance the performance on these benchmarks. Besides, the efficiency is further improved. Note that since the visual tokens removed by the text-guided sampler still go through several layers of computation, the number of remaining tokens is calculated through conversion. Suppose there are m visual tokens and text-guided sampler removes n tokens in i -th layer, then the number of remaining tokens is calculated through $m - n + i * n / 32$, where 32 is the total number of layers.

More scales. In this part, we investigate the effect of additional scales. Building upon the original three scales, 4x4, 2x2, and 1x1, we add four asymmetric scales: 4x2, 2x4,

Table 3. **More flexible pooling designs.** * denotes default.

Setting	TextVQA	MME	ScienceQA	GQA
Baseline	65.5	1562	76.4	61.7
3-branch*	65.2	1590	77.8	62.3
7-branch	66.6	1589	77.2	62.4

2x1, and 1x2. The results are presented in Tab. 3. Here, “Baseline” refers to our reproduction of the LLaVA-Next, “3-Branch” represents the default implementation of our method, and “7-Branch” indicates the extension to 7 visual scales. The results show that adding more scales leads to a notable 1.1% increase in TextVQA over the “3-branch”. We attribute this enhancement to the fact that the TextVQA task requires the recognition of fine-grained information, such as text, and the inclusion of more scales aids the model in better handling these detailed elements.

Window size of feature block In this part, we compare the impact of different window size of feature block in the vision-guided sampler. In the default setting, the feature block size is 4x4. We add several sizes for comparison, including 1x1, 2x2, 8x8, and 12x12. For the 1x1 feature block, since it is no longer possible to perform multi-scale down-sampling, we directly predict whether it should be retained or discarded. For the 2x2 feature block, only 1x1 and 2x2 scales can be used for down-sampling. For 8x8 and 12x12, the down-sampling branches used are consistent with the default configuration. The experimental results are shown in Tab. 4. The results indicate that setting the window size too small or too large is harmful to performance. Window size such as 1x1 and 2x2, even leads to a decrease in performance compared to the baseline. Overall, selecting 4x4 as the feature block size yields the best performance. We believe that as the feature map size decreases, the re-

Table 4. **Influence of size of the local feature block.** * denotes default.

Setting	TextVQA	MME	ScienceQA	GQA
baseline	65.5	1562	76.4	61.7
1x1	64.5	1557	73.9	61.9
2x2	65.1	1549	76.1	61.7
4x4*	65.2	1590	77.8	62.3
8x8	64.9	1570	77.2	61.8
12x12	64.2	1567	78.2	61.5

gions are divided more finely, but the number of available multi-scale options also decreases. Conversely, as the size increases, the region division becomes coarser, and when the scale reaches the same size as the feature map, all regions are down-sampled in the same manner.

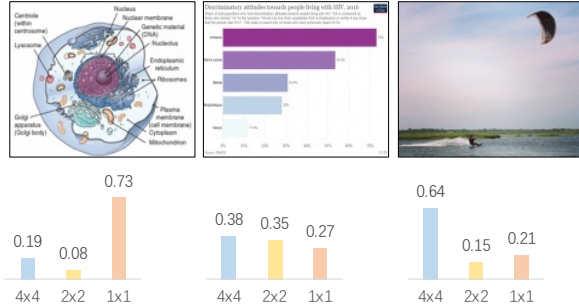


Figure 3. Statistics of multi-scale sampling. For each sample, the proportion of the three types of max-pooling is shown.

Role of balance loss. In this part, we investigate the role of the balance loss in multi-scale selection. The original balance loss is designed to ensure that each expert is selected uniformly in MoE structure. In our scenario, the balance loss encourages the model to explore different visual scale selections, thereby training the sampler module. It is important to note that after being trained with the balance loss, the model does not uniformly select each scale. It adjusts according to the actual situation. For example, as shown in Fig. 3, the proportion of different visual scales chosen by the model varies. In the leftmost image, which contains a lot of text detail, a higher proportion is allocated to 1x1 pooling, meaning no down-sampling is performed. Conversely, in the rightmost image, which has large background areas, a greater proportion is assigned to 4x4 pooling. To further analyze the effect of the balance loss, we conducted an ablation study, and the results are presented in Tab. 5. Based on the results, we find that the setting without balance loss get poor results. We dig deep and find that the selector degrades to consistently select a single scale. For example, if the selector is initialized to select one scale, then this choice won’t be changed during training.

Effect of textual guidance. In this part, we explore the

Table 5. **Role of load balance loss.** * denotes default.

Setting	TextVQA	MME	ScienceQA	GQA
w/o	61.9	1439	74.6	57.1
weight 0.01	63.7	1537	75.9	60.0
weight 0.1*	65.2	1590	77.8	62.3
weight 0.5	65.0	1576	76.9	61.5

Table 6. **Impact of textual guidance.** * denotes default.

Setting	TextVQA	MME	ScienceQA	GQA
Baseline	65.5	1562	76.4	61.7
Direct	64.9	1543	76.6	60.8
Train	65.3	1586	77.3	61.9
Random*	65.4	1603	76.9	62.1

effect of textual guidance. We set up four settings in our experiments. (1) Baseline: train using the original structure of LLaVA-Next. (2) Direct: Based on the baseline, use the text-guided sampler without training. γ is set to 90%. (3) Train: Perform the full Instruction-Tuning with text-guided sampler. (4) Random: Based on “Train”, add augmentation to the layers and γ values. The results are presented in Tab. 6. We observe that using textual guidance without training leads to a noticeable performance drop on the TextVQA, MME, and GQA. After training, the introduction of the Text-guided Filter hardly causes any performance reduction, and even shows slight improvements on MME, ScienceQA, and GQA. With the introduction of the random training technique, we observe clear improvements over the Baseline on MME and GQA. These experimental results indicate that incorporating the training process significantly mitigates the performance drop caused by the text-guided sampler, and our introduced random training technique further enhances the robustness of the process.

Textual guidance in different layers. We investigated the impact of placing a text-guided sampler at different layers within a LLM. The results are presented in Figure-2. Notably, positioning the sampler at the layer 31, which is the final layer of the LLM, is equivalent to not performing any reduction operation. Our findings reveal that as the layer number increases, the model’s inference speed gradually decreases. The model’s performance initially improves before eventually decline. This suggests that the text-guided sampler performs better when placed in the middle layers, aligning with our initial expectations.

What has been selected? In this part, we discuss the roles of the vision-guided sampler and the text-guided sampler in the selection of visual tokens. We have selected several cases to observe the critical regions chosen by each module, with the results illustrated in Fig. 4. For vision-guided sampler, we also select some examples to compare their proportion of each scale. It is shown in Fig. 3. The results reveal

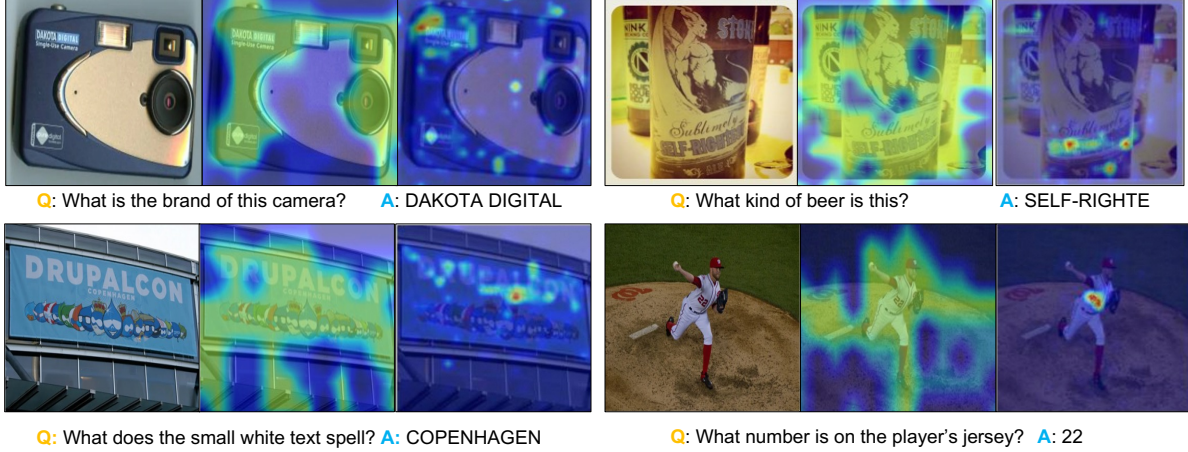


Figure 4. **Heatmap of selected areas from vision-guided sampler and text-guided sampler.** For each image set, from left to right: the original image, the heatmap of vision-guided sampler, the heatmap of text-guided sampler.

that the vision-guided sampler tends to focus on areas of high information density within the image. Specifically, it retains elements such as text, patterns, and people. In contrast, the text-guided sampler emphasizes regions directly related to the query. For instance, when asked about a mobile phone’s brand, it highlights the textual area containing the answer. Similarly, when inquired about the number on a player’s jersey, it disregards most other regions and precisely captures the area where the answer is located.

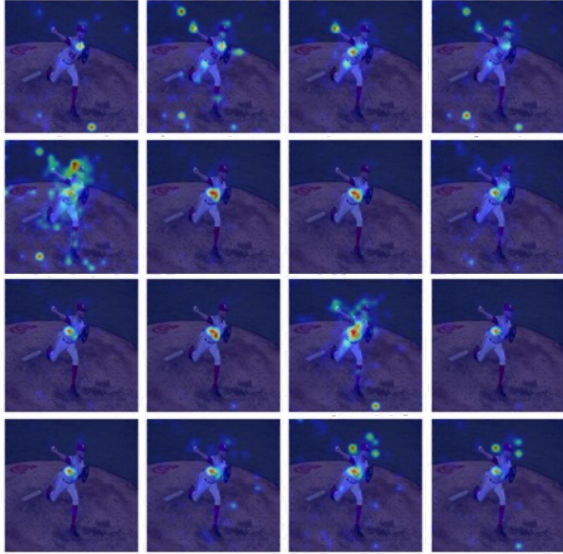


Figure 5. **The importance map from different layers of LLM.** There are 32 layers in total. We select the importance map every two layers. The maps are arranged in reading order.

Evolution of textual guidance. We explore the differences of importance map defined by Eq. (8) across various layers

of the LLM, and the results are presented in Fig. 5. We observed that in the shallow layers of the LLM, textual guidance fails to focus on the regions where the answers are located, and the areas of focus also change frequently. As the layer goes deeper, the regions focused on by textual guidance become increasingly accurate and gradually stabilize. This indicates that the LLM’s understanding of the association between image and text information is a progressive process. Performing filter operations too early will directly discard the image regions containing the answers, thereby affecting the model’s performance, especially in scenarios requiring attention to fine-grained tasks. This also demonstrates the necessity of placing the text-guided sampler in the middle layers of the LLM. On the other hand, since textual guidance in the shallow layers of the LLM is not enough for effectively performing token selection, using visual guidance to remove redundancy before entering LLM is a good complement.

5. Conclusion

In this work, we propose *FocusLLaVA*, which removes visual redundancy adaptively and simultaneously improves both performance and efficiency. *FocusLLaVA* fully leverages both visual and textual information as guidance in its design, forming a coarse-to-fine pipeline for visual token compression. Specifically, it uses visual information to compress redundant regions with low information density and use the textual information to select visual tokens that are strongly correlated with the user instruction. *FocusLLaVA* achieves improvement both in efficiency and performance. Extensive experiments are conducted on various mainstream multimodal benchmarks, to validate the effectiveness of the proposed method.

References

- [1] Jean-Baptiste Alayrac, Jeff Donahue, Pauline Luc, Antoine Miech, Iain Barr, Yana Hasson, Karel Lenc, Arthur Mensch, Katherine Millican, Malcolm Reynolds, Roman Ring, Eliza Rutherford, Serkan Cabi, Tengda Han, Zhitao Gong, Sina Samangooei, Marianne Monteiro, Jacob L. Menick, Sebastian Borgeaud, Andy Brock, Aida Nematzadeh, Sahand Sharifzadeh, Mikolaj Binkowski, Ricardo Barreira, Oriol Vinyals, Andrew Zisserman, and Karén Simonyan. Flamingo: a visual language model for few-shot learning. In *Advances in Neural Information Processing Systems 35: Annual Conference on Neural Information Processing Systems 2022, NeurIPS 2022, New Orleans, LA, USA, November 28 - December 9, 2022*, 2022. 2
- [2] Kazi Hasan Ibn Arif, JinYi Yoon, Dimitrios S Nikolopoulos, Hans Vandierendonck, Deepu John, and Bo Ji. Hired: Attention-guided token dropping for efficient inference of high-resolution vision-language models in resource-constrained environments. *arXiv preprint arXiv:2408.10945*, 2024. 1, 2, 6
- [3] Jinze Bai, Shuai Bai, Shusheng Yang, Shijie Wang, Sinan Tan, Peng Wang, Junyang Lin, Chang Zhou, and Jingren Zhou. Qwen-vl: A versatile vision-language model for understanding, localization, text reading, and beyond. *CoRR*, 2023. 1, 2, 6
- [4] Rohan Bavishi, Erich Elsen, Curtis Hawthorne, Maxwell Nye, Augustus Odena, Arushi Somani, , Sagnak ~ Ta, and srlar. Introducing our multimodal models, 2023. 2
- [5] Mu Cai, Jianwei Yang, Jianfeng Gao, and Yong Jae Lee. Matryoshka multimodal models. *CoRR*, abs/2405.17430, 2024. 1, 2
- [6] Jianjian Cao, Peng Ye, Shengze Li, Chong Yu, Yansong Tang, Jiwen Lu, and Tao Chen. Madtp: Multimodal alignment-guided dynamic token pruning for accelerating vision-language transformer. In *Proceedings of the IEEE/CVF Conference on Computer Vision and Pattern Recognition*, pages 15710–15719, 2024. 2
- [7] Guiming Hardy Chen, Shunian Chen, Ruifei Zhang, Junying Chen, Xiangbo Wu, Zhiyi Zhang, Zhihong Chen, Jianquan Li, Xiang Wan, and Benyou Wang. Allava: Harnessing gpt4v-synthesized data for A lite vision-language model. *CoRR*, abs/2402.11684, 2024. 2
- [8] Guiming Hardy Chen, Shunian Chen, Ruifei Zhang, Junying Chen, Xiangbo Wu, Zhiyi Zhang, Zhihong Chen, Jianquan Li, Xiang Wan, and Benyou Wang. Allava: Harnessing gpt4v-synthesized data for a lite vision-language model, 2024. 5
- [9] Jiaqi Chen, Jianheng Tang, Jinghui Qin, Xiaodan Liang, Lingbo Liu, Eric Xing, and Liang Lin. Geoqa: A geometric question answering benchmark towards multimodal numerical reasoning. In *Findings of the Association for Computational Linguistics: ACL-IJCNLP 2021*, pages 513–523, 2021. 5
- [10] Kezhen Chen, Rahul Thapa, Rahul Chalamala, Ben Athiwaratkun, Shuaiwen Leon Song, and James Zou. Dragonfly: Multi-resolution zoom supercharges large visual-language model. *arXiv preprint arXiv:2406.00977*, 2024. 2
- [11] Lin Chen and Long Xing. Open-llava-next: An open-source implementation of llava-next series for facilitating the large multi-modal model community. <https://github.com/xiaoachen98/Open-LLaVA-NeXT>, 2024. 5
- [12] Lin Chen, Jisong Li, Xiaoyi Dong, Pan Zhang, Conghui He, Jiaqi Wang, Feng Zhao, and Dahua Lin. Sharegpt4v: Improving large multi-modal models with better captions. *arXiv preprint arXiv:2311.12793*, 2023. 5
- [13] Liang Chen, Haozhe Zhao, Tianyu Liu, Shuai Bai, Junyang Lin, Chang Zhou, and Baobao Chang. An image is worth 1/2 tokens after layer 2: Plug-and-play inference acceleration for large vision-language models. *CoRR*, abs/2403.06764, 2024. 2
- [14] Wenliang Dai, Junnan Li, Dongxu Li, Anthony Meng Huat Tiong, Junqi Zhao, Weisheng Wang, Boyang Li, Pascale Fung, and Steven C. H. Hoi. Instructblip: Towards general-purpose vision-language models with instruction tuning. In *Advances in Neural Information Processing Systems 36: Annual Conference on Neural Information Processing Systems 2023, NeurIPS 2023, New Orleans, LA, USA, December 10 - 16, 2023*, 2023. 2, 6
- [15] Alexey Dosovitskiy, Lucas Beyer, Alexander Kolesnikov, Dirk Weissenborn, Xiaohua Zhai, Thomas Unterthiner, Mostafa Dehghani, Matthias Minderer, Georg Heigold, Sylvain Gelly, Jakob Uszkoreit, and Neil Houlsby. An image is worth 16x16 words: Transformers for image recognition at scale. In *International Conference on Learning Representations*, 2021. 2
- [16] William Fedus, Barret Zoph, and Noam Shazeer. Switch transformers: Scaling to trillion parameter models with simple and efficient sparsity. *Journal of Machine Learning Research*, 23(120):1–39, 2022. 4
- [17] Chaoyou Fu, Peixian Chen, Yunhang Shen, Yulei Qin, Mengdan Zhang, Xu Lin, Zhenyu Qiu, Wei Lin, Jinrui Yang, Xiaowu Zheng, Ke Li, Xing Sun, and Rongrong Ji. MME: A comprehensive evaluation benchmark for multimodal large language models. *CoRR*, abs/2306.13394, 2023. 5, 6
- [18] Wenbo Hu, Zi-Yi Dou, Liunian Harold Li, Amita Kamath, Nanyun Peng, and Kai-Wei Chang. Matryoshka query transformer for large vision-language models. *CoRR*, abs/2405.19315, 2024. 2
- [19] Wenbo Hu, Yifan Xu, Yi Li, Weiyue Li, Zeyuan Chen, and Zhuowen Tu. Bliva: A simple multimodal llm for better handling of text-rich visual questions. In *Proceedings of the AAAI Conference on Artificial Intelligence*, pages 2256–2264, 2024. 2
- [20] Drew A. Hudson and Christopher D. Manning. GQA: A new dataset for real-world visual reasoning and compositional question answering. In *IEEE Conference on Computer Vision and Pattern Recognition, CVPR 2019, Long Beach, CA, USA, June 16-20, 2019*, pages 6700–6709. Computer Vision Foundation / IEEE, 2019. 5
- [21] Kushal Kafle, Scott Cohen, Brian Price, and Christopher Kanan. Dvqa: Understanding data visualizations via question answering. In *CVPR*, 2018. 5
- [22] Aniruddha Kembhavi, Mike Salvato, Eric Kolve, Min Joon Seo, Hannaneh Hajishirzi, and Ali Farhadi. A diagram is

- worth a dozen images. In *Computer Vision - ECCV 2016 - 14th European Conference, Amsterdam, The Netherlands, October 11-14, 2016, Proceedings, Part IV*, pages 235–251. Springer, 2016. 5
- [23] Geewook Kim, Teakgyu Hong, Moonbin Yim, JeongYeon Nam, Jinyoung Park, Jinyeong Yim, Wonseok Hwang, Sangdoo Yun, Dongyoon Han, and Seunghyun Park. Ocr-free document understanding transformer. In *Computer Vision - ECCV 2022 - 17th European Conference, Tel Aviv, Israel, October 23-27, 2022, Proceedings, Part XXVIII*, pages 498–517. Springer, 2022. 5
- [24] Bo Li, Peiyuan Zhang, Jingkang Yang, Yuanhan Zhang, Fanyi Pu, and Ziwei Liu. Otterhd: A high-resolution multi-modality model. *CoRR*, abs/2311.04219, 2023. 2, 6
- [25] Junnan Li, Dongxu Li, Silvio Savarese, and Steven C. H. Hoi. BLIP-2: bootstrapping language-image pre-training with frozen image encoders and large language models. In *International Conference on Machine Learning, ICML 2023, 23-29 July 2023, Honolulu, Hawaii, USA*, pages 19730–19742. PMLR, 2023. 1, 2
- [26] Yifan Li, Yifan Du, Kun Zhou, Jinpeng Wang, Wayne Xin Zhao, and Ji-Rong Wen. Evaluating object hallucination in large vision-language models. In *Proceedings of the 2023 Conference on Empirical Methods in Natural Language Processing, EMNLP 2023, Singapore, December 6-10, 2023*, pages 292–305. Association for Computational Linguistics, 2023. 5
- [27] Yanwei Li, Yuechen Zhang, Chengyao Wang, Zhisheng Zhong, Yixin Chen, Ruihang Chu, Shaoteng Liu, and Jiaya Jia. Mini-gemini: Mining the potential of multi-modality vision language models. *CoRR*, abs/2403.18814, 2024. 2, 6
- [28] Zhang Li, Biao Yang, Qiang Liu, Zhiyin Ma, Shuo Zhang, Jingxu Yang, Yabo Sun, Yuliang Liu, and Xiang Bai. Monkey: Image resolution and text label are important things for large multi-modal models. In *Proceedings of the IEEE/CVF Conference on Computer Vision and Pattern Recognition (CVPR)*, pages 26763–26773, 2024. 1, 2
- [29] Bin Lin, Zhenyu Tang, Yang Ye, Jiayi Cui, Bin Zhu, Peng Jin, Junwu Zhang, Munan Ning, and Li Yuan. Moe-llava: Mixture of experts for large vision-language models. *CoRR*, abs/2401.15947, 2024. 2
- [30] Chen Lin and Xing Long. Open-llava-next: An open-source implementation of llava-next series for facilitating the large multi-modal model community. <https://github.com/xiaoachen98/Open-LLaVA-NeXT>, 2024. 2, 3, 5
- [31] Ziyi Lin, Chris Liu, Renrui Zhang, Peng Gao, Longtian Qiu, Han Xiao, Han Qiu, Chen Lin, Wenqi Shao, Keqin Chen, Jiaming Han, Siyuan Huang, Yichi Zhang, Xuming He, Hongsheng Li, and Yu Qiao. SPHINX: the joint mixing of weights, tasks, and visual embeddings for multi-modal large language models. *CoRR*, abs/2311.07575, 2023. 2
- [32] Zhihang Lin, Mingbao Lin, Luxi Lin, and Rongrong Ji. Boosting multimodal large language models with visual tokens withdrawal for rapid inference. *CoRR*, abs/2405.05803, 2024. 2
- [33] Haotian Liu, Chunyuan Li, Qingyang Wu, and Yong Jae Lee. Visual instruction tuning. In *Advances in Neural Information Processing Systems 36: Annual Conference on Neural Information Processing Systems 2023, NeurIPS 2023, New Orleans, LA, USA, December 10 - 16, 2023*, 2023. 1, 2, 5
- [34] Haotian Liu, Chunyuan Li, Yuheng Li, and Yong Jae Lee. Improved baselines with visual instruction tuning. In *Proceedings of the IEEE/CVF Conference on Computer Vision and Pattern Recognition (CVPR)*, pages 26296–26306, 2024. 1, 2, 6
- [35] Haotian Liu, Chunyuan Li, Yuheng Li, Bo Li, Yuanhan Zhang, Sheng Shen, and Yong Jae Lee. Llava-next: Improved reasoning, ocr, and world knowledge, 2024. 2, 5, 6
- [36] Yuan Liu, Haodong Duan, Yuanhan Zhang, Bo Li, Songyang Zhang, Wangbo Zhao, Yike Yuan, Jiaqi Wang, Conghui He, Ziwei Liu, Kai Chen, and Dahua Lin. Mmbench: Is your multi-modal model an all-around player? *CoRR*, abs/2307.06281, 2023. 5, 6
- [37] Yuliang Liu, Biao Yang, Qiang Liu, Zhang Li, Zhiyin Ma, Shuo Zhang, and Xiang Bai. Textmonkey: An ocr-free large multimodal model for understanding document. *CoRR*, abs/2403.04473, 2024. 2
- [38] Pan Lu, Swaroop Mishra, Tanglin Xia, Liang Qiu, Kai-Wei Chang, Song-Chun Zhu, Oyvind Tafjord, Peter Clark, and Ashwin Kalyan. Learn to explain: Multimodal reasoning via thought chains for science question answering. In *Advances in Neural Information Processing Systems 35: Annual Conference on Neural Information Processing Systems 2022, NeurIPS 2022, New Orleans, LA, USA, November 28 - December 9, 2022*, 2022. 5, 6
- [39] Gen Luo, Yiyi Zhou, Yuxin Zhang, Xiawu Zheng, Xiaoshuai Sun, and Rongrong Ji. Feast your eyes: Mixture-of-resolution adaptation for multimodal large language models. *arXiv preprint arXiv:2403.03003*, 2024. 2
- [40] Ahmed Masry, Do Xuan Long, Jia Qing Tan, Shafiq R. Joty, and Enamul Hoque. Chartqa: A benchmark for question answering about charts with visual and logical reasoning. In *Findings of the Association for Computational Linguistics: ACL 2022, Dublin, Ireland, May 22-27, 2022*, pages 2263–2279. Association for Computational Linguistics, 2022. 5
- [41] Minesh Mathew, Dimosthenis Karatzas, and C. V. Jawahar. Docvqa: A dataset for VQA on document images. In *IEEE Winter Conference on Applications of Computer Vision, WACV 2021, Waikoloa, HI, USA, January 3-8, 2021*, pages 2199–2208. IEEE, 2021. 5
- [42] Alec Radford, Jong Wook Kim, Chris Hallacy, Aditya Ramesh, Gabriel Goh, Sandhini Agarwal, Girish Sastry, Amanda Askell, Pamela Mishkin, Jack Clark, Gretchen Krueger, and Ilya Sutskever. Learning transferable visual models from natural language supervision. In *Proceedings of the 38th International Conference on Machine Learning, ICML 2021, 18-24 July 2021, Virtual Event*, pages 8748–8763. PMLR, 2021. 5
- [43] Yuzhang Shang, Mu Cai, Bingxin Xu, Yong Jae Lee, and Yan Yan. Llava-prumerge: Adaptive token reduction for efficient large multimodal models. *CoRR*, abs/2403.15388, 2024. 2, 6
- [44] Amanpreet Singh, Vivek Natarajan, Meet Shah, Yu Jiang, Xinlei Chen, Dhruv Batra, Devi Parikh, and Marcus

- Rohrbach. Towards VQA models that can read. In *IEEE Conference on Computer Vision and Pattern Recognition, CVPR 2019, Long Beach, CA, USA, June 16-20, 2019*, pages 8317–8326, 2019. [5](#), [6](#)
- [45] Dingjie Song, Wenjun Wang, Shunian Chen, Xidong Wang, Michael Guan, and Benyou Wang. Less is more: A simple yet effective token reduction method for efficient multi-modal llms. *arXiv preprint arXiv:2409.10994*, 2024. [1](#), [2](#), [6](#)
- [46] Peng Wang, Shuai Bai, Sinan Tan, Shijie Wang, Zhihao Fan, Jinze Bai, Keqin Chen, Xuejing Liu, Jialin Wang, Wenbin Ge, et al. Qwen2-vl: Enhancing vision-language model’s perception of the world at any resolution. *arXiv preprint arXiv:2409.12191*, 2024. [2](#)
- [47] Haoran Wei, Lingyu Kong, Jinyue Chen, Liang Zhao, Zheng Ge, Jinrong Yang, Jianjian Sun, Chunrui Han, and Xiangyu Zhang. Vary: Scaling up the vision vocabulary for large vision-language models. *CoRR*, abs/2312.06109, 2023. [2](#)
- [48] Ruyi Xu, Yuan Yao, Zonghao Guo, Junbo Cui, Zanlin Ni, Chunjiang Ge, Tat-Seng Chua, Zhiyuan Liu, Maosong Sun, and Gao Huang. Llava-uhd: an lmm perceiving any aspect ratio and high-resolution images. *arXiv preprint arXiv:2403.11703*, 2024. [2](#)
- [49] Jiabo Ye, Haiyang Xu, Haowei Liu, Anwen Hu, Ming Yan, Qi Qian, Ji Zhang, Fei Huang, and Jingren Zhou. mplug-owl3: Towards long image-sequence understanding in multi-modal large language models. *arXiv preprint arXiv:2408.04840*, 2024. [6](#)
- [50] Weihao Yu, Zhengyuan Yang, Linjie Li, Jianfeng Wang, Kevin Lin, Zicheng Liu, Xinchao Wang, and Lijuan Wang. Mm-vet: Evaluating large multimodal models for integrated capabilities. In *Forty-first International Conference on Machine Learning*, 2024. [5](#)
- [51] Ya-Qi Yu, Minghui Liao, Jihao Wu, Yongxin Liao, Xiaoyu Zheng, and Wei Zeng. Texthawk: Exploring efficient fine-grained perception of multimodal large language models. *arXiv preprint arXiv:2404.09204*, 2024. [1](#), [2](#)
- [52] Ya-Qi Yu, Minghui Liao, Jiwen Zhang, and Jihao Wu. Texthawk2: A large vision-language model excels in bilingual ocr and grounding with 16x fewer tokens. *arXiv preprint arXiv:2410.05261*, 2024. [2](#)
- [53] Renshan Zhang, Yibo Lyu, Rui Shao, Gongwei Chen, Weili Guan, and Liqiang Nie. Token-level correlation-guided compression for efficient multimodal document understanding. *arXiv preprint arXiv:2407.14439*, 2024. [2](#)
- [54] Yi-Fan Zhang, Qingsong Wen, Chaoyou Fu, Xue Wang, Zhang Zhang, Liang Wang, and Rong Jin. Beyond llava-hd: Diving into high-resolution large multimodal models. *arXiv preprint arXiv:2406.08487*, 2024. [1](#), [2](#), [6](#)

FocusLLaVA: A Coarse-to-Fine Approach for Efficient and Effective Visual Token Compression

Supplementary Material

6. Comparison with Heuristic Visual Token Dropping

In this part, we compare the proposed method with the manually designed metrics. This is used to illustrate that a learned metric rather than hand-crafted will solve the problem of performance reduction. To this end, we modify the vision-guided sampler by removing its mechanism for predicting scales and instead select important tokens based on manually designed similarity measures. Specifically, for each feature block, we flatten it to obtain $\mathbf{X}_i \in \mathbb{R}^{16 \times C}$, and then compute the similarity matrix with the global image feature block $\mathbf{X}_g \in \mathbb{R}^{H_x W_x \times C}$ to get $A_i = \mathbf{X}_g^T \mathbf{X}_i \in \mathbb{R}^{H_x W_x \times 16}$. We then calculate the importance score for each token in the feature block by averaging: $Score_i = \frac{1}{H_x W_x} \sum_{j=1}^{H_x W_x} A_{ij}$. Finally, we concatenate all $Score_i$ and select the top visual tokens based on these scores. Our experimental results, as shown in Tab. 7, indicate that using manually designed methods leads to a decrease in model performance, regardless of the number of visual tokens retained. In contrast, FocusLLaVa achieves performance improvements even when reducing the number of visual tokens.

Table 7. Comparison with heuristic methods.

Setting	#Visual Tokens	TextVQA	MME	ScienceQA	GQA
Top-100%	100%	65.5	1562	76.4	61.7
Top-80%	80%	65.2	1571	76.2	61.3
Top-60%	60%	64.3	1549	75.9	58.9
Top-40%	40%	62.6	1508	75.2	58.4
FocusLLaVa	49%	65.2	1590	77.8	62.3

7. More Examples

In this part, more examples are visualized in Fig. 6 and Fig. 7 to demonstrate the different characteristics of visual guidance and textual guidance. Besides, we also visualize the different areas selected across different instructions. It is shown in Fig. 8 and Fig. 9.

8. Details of the Evolution of Textual Guidance

In this part, we further analyze the evolution of textual guidance as the number of layers increases. In Fig. 10, the question posed is "What number is on the player's jersey?". Our analysis reveals that the textual guidance does not immediately focus on the answer region but rather evolves systematically. Initially, the model focuses on the player and some

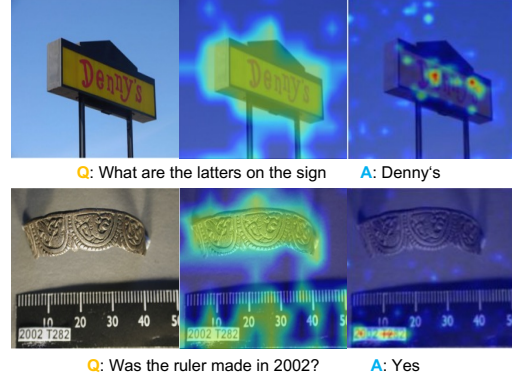


Figure 6. Selected areas from vision-guided sampler and text-guided sampler.



Figure 7. Selected areas from vision-guided sampler and text-guided sampler.

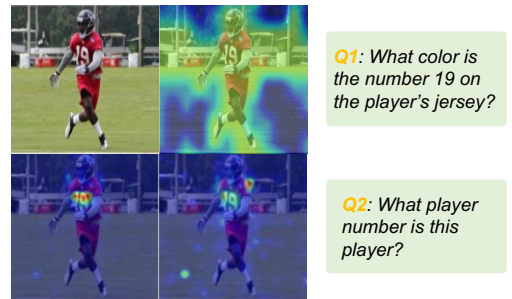


Figure 8. Difference of selected areas across different queries.

irrelevant areas in the image. Subsequently, it shifts its attention to the entire body of the player, including the limbs and the clothing. The model then begins to concentrate on

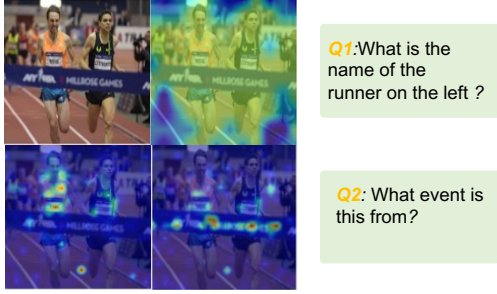


Figure 9. **Difference of selected areas across different queries.**

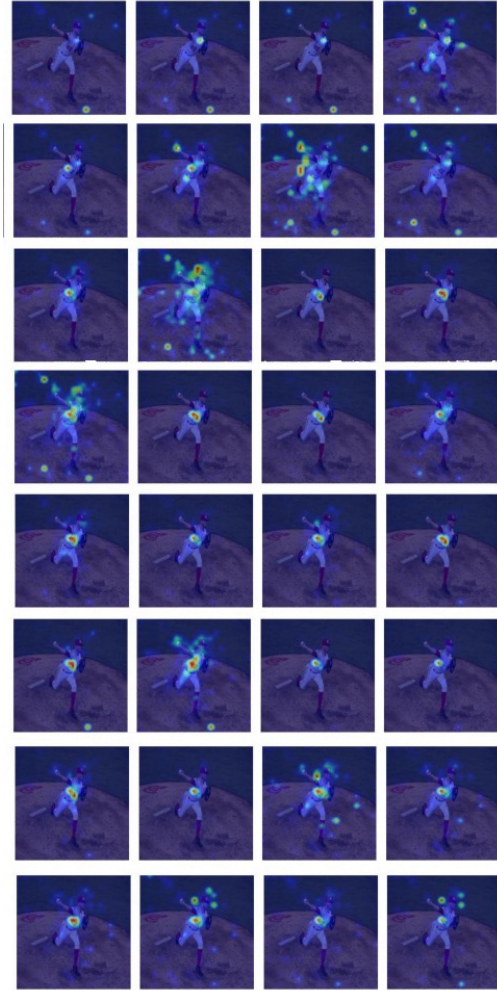


Figure 10. **Full details of the evolution of textual guidance across LLM layers.**

the number on the clothing. However, after initially focusing on the numbers, the model does not maintain a consistent focus; instead, it intermittently returns its attention to the player and the clothing. Starting from the 8th layer, the model consistently focuses on the number region, although

there are still occasional shifts in attention to other areas. This process can be interpreted as the model continuously refining its reasoning and adjusting its focus, even revisiting and reconfirming previously identified regions, until it stabilizes on the correct answer.

9. Imbalance Loss

In this section, we further investigate the impact of balance loss on model performance. During our training process, under the constraint of balance loss, the model is required to select three different visual scales with as equal probability as possible. We believe that in real-world scenarios, different situations may have a preference for a particular visual scale. Therefore, by modifying the form of the balance loss, we constructed an imbalance loss to adjust the model’s preferences. Specifically, we add coefficients to each scale, making the loss function as follows:

$$L_{\text{imbalance}} = \alpha \sum_{i=0}^n w_i f_i P_i, \quad (10)$$

where w_i represents the penalty coefficient for the i -th branch. To align with the original loss values, w_i must satisfy $\sum_{i=0}^n w_i = 3$. For the balance loss, $w_i = 1$, meaning the coefficients for all branches are the same. Increasing w_i means increasing the penalty for that branch, leading the model to be less likely to choose it. Conversely, decreasing w_i makes the model more inclined to select that branch. The results are shown in Tab. 8, where the list under “setting” in the table represents the penalty coefficients for the three branches, corresponding to 1x1 pooling, 2x2 pooling, and 4x4 pooling, respectively. We find that when the penalty coefficient for 1x1 pooling is increased, the model tends to perform more downsampling operations, which significantly degrades its performance on TextVQA. Conversely, decreasing the penalty coefficient for 1x1 pooling improves the model’s performance on TextVQA. The ScienceQA test set is also affected, but with a completely opposite trend. We believe this is due to the differences in the tasks of the test sets. TextVQA requires the model to focus on text-related factual details in images, so a preference for finer scales is beneficial. In contrast, ScienceQA demands more reasoning from the model and does not require as much attention to the fine details of the image.

Table 8. **Exploration of imbalance loss.**

Setting	TextVQA	MME	ScienceQA	GQA
Baseline	65.5	1562	76.4	61.7
[1.0, 1.0, 1.0]	65.2	1590	77.8	62.3
[1.1, 1.0, 0.9]	63.7	1581	78.0	61.1
[0.9, 1.0, 1.1]	65.7	1587	76.1	62.1